The 4D Hyperspherical Diffusion Wavelet: A New Method for the Detection of Localized Anatomical Variation

Ameer Pasha Hosseinbor[1], Won Hwa Kim[1], Nagesh Adluru[1], Amit Acharya[2], Houri K. Vorperian[1], and Moo K. Chung[1]

[1] University of Wisconsin-Madison, USA
[2] Marshfield Clinic, USA
hosseinbor@wisc.edu

Abstract. Recently, the HyperSPHARM algorithm was proposed to parameterize multiple disjoint objects in a holistic manner using the 4D hyperspherical harmonics. The HyperSPHARM coefficients are global; they cannot be used to directly infer localized variations in signal. In this paper, we present a unified wavelet framework that links HyperSPHARM to the diffusion wavelet transform. Specifically, we will show that the HyperSPHARM basis forms a subset of a wavelet-based multiscale representation of surface-based signals. This wavelet, termed the hyperspherical diffusion wavelet, is a consequence of the equivalence of isotropic heat diffusion smoothing and the diffusion wavelet transform on the hypersphere. Our framework allows for the statistical inference of highly localized anatomical changes, which we demonstrate in the first-ever developmental study on the hyoid bone investigating gender and age effects. We also show that the hyperspherical wavelet successfully picks up group-wise differences that are barely detectable using SPHARM.

1 Introduction

Studying and quantifying the development of anatomical structures over time is important in medical image analysis. Anatomical development tends to exhibit highly localized, complex growth [9]. Unfortunately, existing surface-based morphometric techniques are based on global bases, and thus are unable to detect subtle localized anatomical variations. For anatomical developmental studies, there is then a real need for surface-based approaches with localization power.

Recently, the HyperSPHARM algorithm [7] was proposed to parameterize multiple disjoint structures (e.g. hyoid bone) in a holistic manner. The underlying idea behind HyperSPHARM is to stereographically project n-dimensional data onto the $(n+1)$-dimensional hypersphere and subsequenly parameterize it with the $(n+1)$-dimensional hyperspherical harmonics (HSH). As with SPHARM [5,8], the HyperSPHARM coefficients are global, so if they exhibit statistical differences, interpreting which anatomical regions contribute to these variations is difficult. Consequently, the HyperSPHARM coefficients cannot be used directly

P. Golland et al. (Eds.): MICCAI 2014, Part III, LNCS 8675, pp. 65–72, 2014.
© Springer International Publishing Switzerland 2014

to infer localized variations in signal. Although this fact may seem to render HyperSPHARM as a purely global inference algorithm, HyperSPHARM is actually a feature of wavelet localization.

In this paper, a unified wavelet framework is developed that links HyperSPHARM to the diffusion wavelet transform [4]. Specifically, we will show that the HyperSPHARM basis forms a subset of a wavelet-based multi-scale representation of surface-based signals. We will derive this wavelet, which we term the hyperspherical diffusion wavelet. Our framework allows for the statistical inference of highly localized anatomical changes, which we demonstrate in a developmental study on the hyoid bone investigating gender and age effects. We will also show that the hyperspherical wavelet outperforms SPHARM in detecting group-wise differences.

2 Theory

In this section, we will briefly review HyperSPHARM, before deriving the hyperspherical wavelet and its corresponding coefficients.

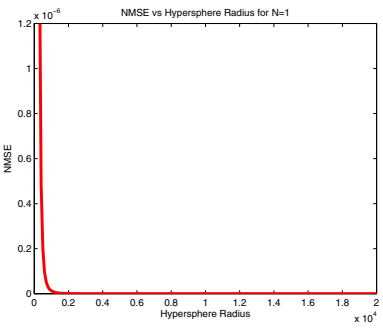

Fig. 1. NMSE versus hypersphere radius for N=1 HSH recon of hyoid template

4D Hyperspherical Harmonics
Consider the 4D unit hypersphere S^3 existing in $\mathbb{R}^4$. The Laplace-Beltrami operator on S^3 is defined as $\Delta_{S^3} = \frac{1}{\sin^2\beta}\frac{\partial}{\partial\beta}\sin^2\beta\frac{\partial}{\partial\beta} + \frac{1}{\sin^2\beta}\Delta_{S^2}$, where Δ_{S^2} is the Laplace-Beltrami operator on the unit sphere S^2. The eigenfuctions of Δ_{S^3} are the 4D HSH $Z_{nl}^m(\beta,\theta,\phi)$: $\Delta_{S^3}Z_{nl}^m = -l(l+2)Z_{nl}^m$, and we refer the reader to [7] for their exact functional form. The hyperspherical angles (β,θ,ϕ) obey $(\beta\in[0,\pi],\theta\in[0,\pi],\phi\in[0,2\pi])$, and the three integers (n,l,m) obey the conditions $n=0,1,2,...,\ 0\le l\le n$, and $-l\le m\le l$. The 4D HSH form an orthonormal basis on S^3.

Isotropic Heat Diffusion Smoothing on 4D Hypersphere
Consider an arbitrary 3D manifold $\mathcal{M}\subset\mathbb{R}^3$ defined by surface coordinates $\mathbf{q}=(q,\theta,\phi)$, and some real-valued functional measurement $f(\mathbf{q})$ defined on the manifold. The manifold $\mathcal{M}$ can be either multiple disjoint components such as the hyoid bone, or a single connected component. We stereographically project the 3D manifold onto a 4D hypersphere of radius r_o in $\mathbb{R}^4$, whose coordinates are denoted by the vector $\mathbf{u}=(\beta,\theta,\phi)$. Consequently, the functional measurement f exists along the surface of the 4D hypersphere. Note that the measurement $f(\mathbf{q})$ on $\mathcal{M}$ is equivalent to its corresponding projection $f(\mathbf{u})$ on the hypersphere.

We assume that $f(\mathbf{u})$ is square-integrable along the surface of the hypersphere. According to Fourier analysis, any square-integrable function defined on

a sphere can be expanded in terms of the spherical harmonics. Thus, $f(\mathbf{u})$ can be expanded in terms of the 4D HSH:

$$f(\mathbf{u}) = \sum_{n=0}^{N} \sum_{l=0}^{n} \sum_{m=-l}^{l} C_{nlm} Z_{nl}^{m}(\mathbf{u}), \tag{1}$$

where N is the truncation order of the HSH expansion. Eq. (1) is simply the HyperSPHARM basis.

Now lets have $f(\mathbf{u})$ undergo isotropic heat diffusion smoothing. We want to determine the function $K(\mathbf{u}, t)$ that describes the variation of $f(\mathbf{u})$ with respect to smoothing parameter t. Naturally, when no smoothing is applied, i.e. $t = 0$, we have $K(\mathbf{u}, 0) = f(\mathbf{u})$. The function $K(\mathbf{u}, t)$ is then a solution to the isotropic heat equation on the 4D hypersphere, subject to the aforementioned initial condition:

$$\frac{\partial}{\partial t} K(\mathbf{u}, t) - \Delta_{S^3} K(\mathbf{u}, t) = 0, \quad K(\mathbf{u}, t = 0) = f(\mathbf{u}) \tag{2}$$

Eq. (2) can be solved analytically by employing an ansatz solution of the form $K(\mathbf{u}, t) = \sum_{n=0}^{\infty} \sum_{l=0}^{n} \sum_{m=-l}^{l} C_{nlm} h_{nlm}(t) Z_{nl}^{m}(\mathbf{u})$, where $h_{nlm}(t)$ is the smoothing term. Upon substituting the ansatz solution into (2), we determine the smoothing term to be $h_l(t) = b_l e^{-l(l+2)t}$. Hence, the solution to Eq. (2) is

$$K(\mathbf{u}, t) = \sum_{n=0}^{N} \sum_{l=0}^{n} \sum_{m=-l}^{l} C_{nlm} e^{-l(l+2)t} Z_{nl}^{m}(\mathbf{u}), \tag{3}$$

where all constants are absorbed into C_{nlm}.

Connection to Diffusion Wavelet

Diffusion wavelets are a multi-scale framework for the analysis of functions on manifolds and graphs [1,6]. Consider the eigenfunctions ψ_j and eigenvalues λ_j on an arbitrary d-dimensional manifold $\mathcal{M}_d$, which satisfy $\Im \psi_j = \lambda_j \psi_j$ for some self-adjoint operator $\Im$ defined on $\mathcal{M}_d$. Following the notations in [1,6], the diffusion wavelet $W_{t,p}(s)$ at position p and scale t characterizing the manifold $\mathcal{M}_d$ is given by

$$W_{t,p}(s) = \sum_{j=0}^{k} g(\lambda_j, t) \psi_j(p) \psi_j(s), \tag{4}$$

where g is some scaling function. The diffusion wavelet coefficients of a given function $\epsilon(s)$ existing on the manifold $\mathcal{M}_d$ is given by the inner product of the wavelets and the given function:

$$\langle W_{t,p}, \epsilon \rangle = \int_M W_{t,p}(s) \epsilon(s) ds \tag{5}$$

If the manifold $\mathcal{M}_d$ is taken to be the 4D hypersphere, then $\Im$ is the Laplace-Beltrami operator on S^3; ψ_j is the 4D HSH basis Z_{nl}^m; and $\lambda_j = -l(l+2)$. Then Eq. (4) becomes

$$\boxed{W_{t,\mathbf{u}}(\mathbf{v}) = \sum_{n=0}^{N} \sum_{l=0}^{n} \sum_{m=-l}^{l} e^{-l(l+2)t} Z_{nl}^m(\mathbf{u}) Z_{nl}^m(\mathbf{v}),} \tag{6}$$

where we have taken $g(\lambda_j, t) = e^{-l(l+2)t}$. Eq. (6) is the 4D hyperspherical diffusion wavelet. Substituting Eqs. (1) and (6) into Eq. (5) gives the hyperspherical wavelet coefficients of any functional measurement f existing on the 4D hypersphere:

$$\boxed{\langle W_{t,\mathbf{u}}, f \rangle = \sum_{n=0}^{N} \sum_{l=0}^{n} \sum_{m=-l}^{l} C_{nlm} e^{-l(l+2)t} Z_{nl}^m(\mathbf{u})} \tag{7}$$

Eq. (7) is equivalent to Eq. (3), i.e. the hyperspherical wavelet coefficients are simply the functional measurement at different smoothing scales, which indicates that isotropic heat diffusion smoothing and the diffusion wavelet transform are identical operations on the hypersphere. It should be noted that a similar 3D analysis will result in the SPHARM wavelet.

3 Application

Numerical Implementation
The numerical implementation follows that of the HyperSPHARM algorithm. The task at hand is to estimate the HSH coefficients C_{nlm} in Eq. (1) for the functional measurement $f = (x^1, x^2, x^3)$, where (x^1, x^2, x^3) are the surface coordinates of the 3D manifold $\mathcal{M}$.

Suppose the manifold $\mathcal{M}$ comprises M mesh vertices, and let $\Omega_j = (\beta_j, \theta_j, \phi_j)$ denote the hyperspherical angles at the j-th mesh vertex. Denote $\mathbf{x}^i$ as the M x 1 vector representing each x^i's M vertices, $\mathbf{C}^i$ the Q x 1 vector of unknown expansion coefficients C_{nlm}^i for each x^i, and $\mathbf{A}$ the M x Q matrix constructed with the HSH basis

$$\mathbf{A} = \begin{pmatrix} Z_{00}^0(\Omega_1) & Z_{10}^0(\Omega_1) & Z_{11}^{-1}(\Omega_1) & Z_{11}^0(\Omega_1) & \cdots & Z_{NN}^N(\Omega_1) \\ \vdots & \vdots & \vdots & \vdots & \ddots & \vdots \\ Z_{00}^0(\Omega_M) & Z_{10}^0(\Omega_M) & Z_{11}^{-1}(\Omega_M) & Z_{11}^0(\Omega_M) & \cdots & Z_{NN}^N(\Omega_M) \end{pmatrix}.$$

Thus, the general linear system representing Eq. (1) is described by $\mathbf{x}^i = \mathbf{A}\mathbf{C}^i$, and is solved via linear least squares, yielding $\widehat{\mathbf{C}^i} = (\mathbf{A}^T\mathbf{A})^{-1}\mathbf{A}^T\mathbf{x}^i$. Once the HyperSPHARM coefficients have been estimated, heat diffusion smoothing is applied to obtain the hyperspherical wavelet coefficients given by Eq. (7).

CT Imaging Data and Preprocessng

The study consists of CT images of 70 normal subjects (33 female and 37 male), whose age range is between 0 and 20 years. Subjects are binned into three age categories: ages between 0 and 6 years (group I), 7 and 12 years (group II), and 13 and 19 years (group III). There are 26, 14, and 30 subjects in groups I, II, and III, respectively. Using this dataset, we seek to address two issues: 1) whether there are any localized hyoid bone growth spurts between these age groups and 2) whether there are any gender differences in the hyoid bone.

The hyoid bone was segmented manually. Correspondence for SPHARM and HyperSPHARM was established in a similar manner as proposed in [3]. The 70 subjects were first affinely aligned so to remove the overall size variablity. Since some subjects may have a larger hyoid bone than others, it is necessary to remove the global size differences in local shape modeling. For this reason, diffeomorphic nonlinear image registration was then performed on the affinely registered template using Advanced Normalization Tools (ANTS) [2]. SPHARM and HyperSPHARM are then used to further register the surfaces via surface flattening and stereographic projection, respectively. Please note this approach avoids the surface alignment done by coinciding the first order ellipsoid meridian and equator proposed in [5].

The HSH truncation order was $N = 1$ and hypersphere radius $r_o = 12000$. The appropriate radius was determined by plotting the mean squared error as a function of radius and selecting the radius that minimized it (Fig. 1). The SPHARM truncation order was $L = 20$. The appropriate wavelet scales t were determined using cluster size inference. The hyperspherical and SPHARM wavelet coefficients are estimated for each vertex at scales $t = [0.01\ 0.05]$ for gender and $t = 0.005$ for age. The SPHARM estimation is special generate case of the SPHARM wavelet at $t = 0$. Hotelling's T^2 test was then carried out at the voxel level at .05 significance level for group analysis with respect to age and gender. The resulting p-value map was corrected for multiple comparisons across all vertices using the false discovery rate (FDR) method.

Hotelling T^2 Statistical Results and Discussion

Only results related to gender and age groups I vs. II are presented. Figs. 2 and 3 summarize the results of our analysis using hyperspherical/SPHARM wavelets and SPHARM, with non-red regions indicating statistical significance. All three methods detect significant gender differences and growth spurts at several regions along the right and left hyoid bones and near the regions that connect the disconnected hyoid bones. SPHARM, however, detects no significant gender and age effects in the middle hyoid bone, unlike the hyperspherical wavelet. The SPHARM wavelet does detect significant gender differences in a few areas along the middle hyoid bone, but no age effects. For both age and gender, the hyperspherical wavelet had the largest number of significant vertices, followed by SPHARM wavelet, and then SPHARM. For gender, the hyperspherical wavelet has a total of 8575 statistically significant vertices, whereas SPHARM wavelet has 6384 and SPHARM 2928. For age, the hyperspherical wavelet detects 5394 statistically significant vertices, followed by SPHARM wavelet with 5330, and SPHARM with 4854.

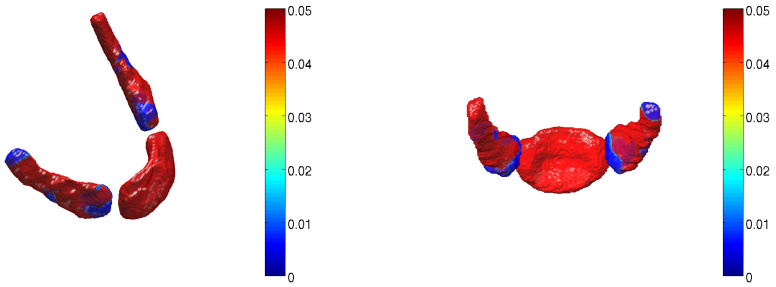

SPHARM: Gender

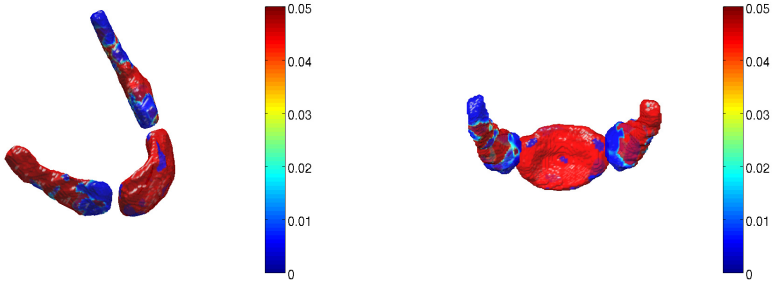

SPHARM Wavelet: Gender

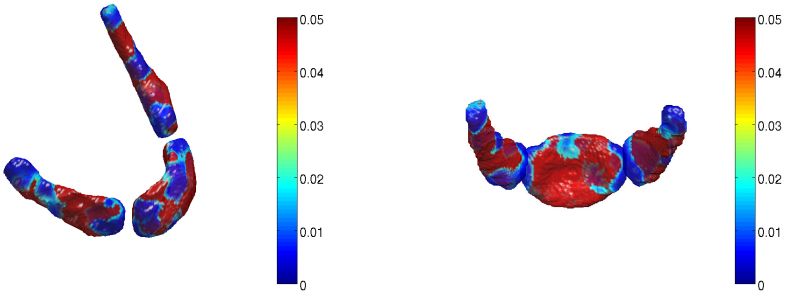

Hyperspherical Wavelet: Gender

Fig. 2. Testing for gender differences. p-values after FDR correction (i.e. q-value), projected back onto hyoid bone template. For hyperspherical wavelet, q-value < 0.028 corresponds to significance; for SPHARM wavelet, q-value < 0.029 (LH), < 0.005 (MH), and < 0.019 (RH); for SPHARM, q-value < 0.011 (LH) and < 0.014 (RH).

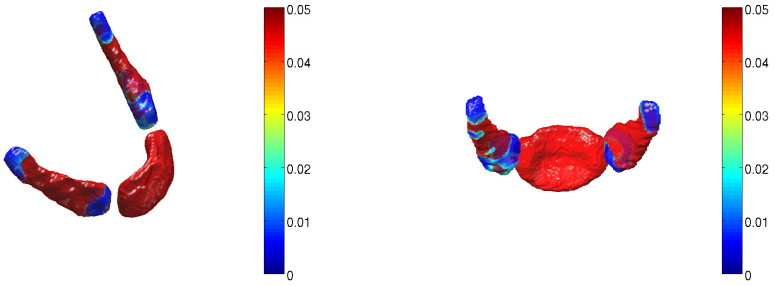

SPHARM: Age Groups I & II

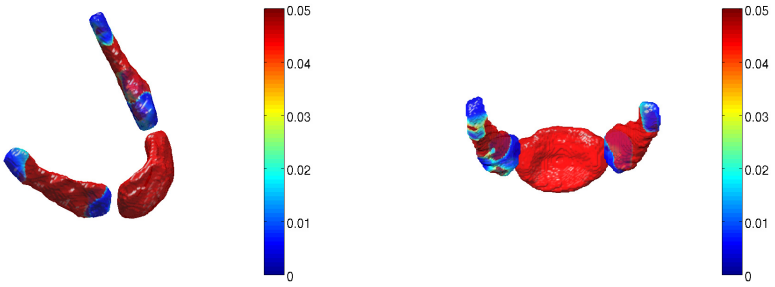

SPHARM Wavelet: Age Groups I & II

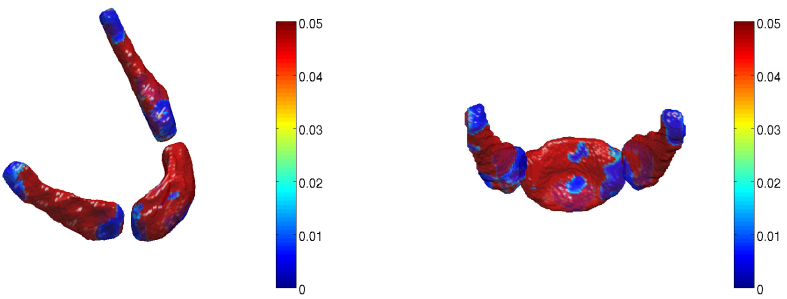

Hyperspherical Wavelet: Age Groups I & II

Fig. 3. Testing for age effects. p-values after FDR correction (i.e. q-value), projected back onto hyoid bone template. For hyperspherical wavelet, q-value < 0.014 corresponds to significance; for SPHARM wavelet, q-value < 0.028 (LH) and < 0.016 (RH); for SPHARM, q-value < 0.026 (LH) and < 0.014 (RH).

The hyperspherical diffusion wavelet's outperformance of SPHARM is due to the wavelet being a local basis whereas SPHARM employs a global basis. The wavelet's inherent localization power, therefore, enables it to infer localized shape variations much better than globally-based methods like SPHARM. SPHARM wavelet's outperformance of SPHARM is for the same reason.

4 Conclusion

In this paper, we have introduced the hyperspherical diffusion wavelet, which allows for the statistical detection of highly localized variations in anatomical morphology. It was used in the first ever developmental study on the hyoid bone, and subsequent statistical testing on the wavelet coefficients revealed localized gender differences and growth spurts in the hyoid bone. We also showed that our framework is more sensitive in signal detection, outperforming both SPHARM wavelet and SPHARM in the discernment of group-wise differences.

Acknowledgements. This research was supported by NIH grants R01DC006282, P30HD003352, and 5T15LM007359, and Vilas Associate Award from UW-Madison.

References

1. Antoine, J.P., Rosca, D., Vandergheynst, P.: Wavelet transform on manifolds: old and new approaches. Applied and Computational Harmonic Analysis 28, 189–202 (2010)
2. Avants, B., Epstein, C., Grossman, M., Gee, J.: Symmetric diffeomorphic image registration with cross-correlation: Evaluating automated labeling of elderly and neurodegenerative brain. Medical Image Analysis 12, 26–41 (2008)
3. Chung, M.K., Dalton, K.M., Shen, L., Evans, A.C., Davidson, R.J.: Weighted Fourier series representation and its application to quantifying the amount of gray matter. IEEE Transac. Med. Imaging 26, 566–581 (2007)
4. Coifman, R., Maggioni, M.: Diffusion wavelets. Applied and Computational Harmonic Analysis 21, 53–94 (2006)
5. Gerig, G., Styner, M., Jones, D., Weinberger, D., Lieberman, J.: Shape analysis of brain ventricles using spharm. In: MMBIA, pp. 171–178 (2001)
6. Hammond, D.K., Vandergheynst, P., Gribonval, R.: Wavelets on graphs via spectral graph theory. Applied and Computational Harmonic Analysis 30, 129–150 (2011)
7. Hosseinbor, A.P., Chung, M.K., Schaefer, S.M., van Reekum, C.M., Peschke-Schmitz, L., Sutterer, M., Alexander, A.L., Davidson, R.J.: 4D hyperspherical harmonic (HyperSPHARM) representation of multiple disconnected brain subcortical structures. In: Mori, K., Sakuma, I., Sato, Y., Barillot, C., Navab, N. (eds.) MICCAI 2013, Part I. LNCS, vol. 8149, pp. 598–605. Springer, Heidelberg (2013)
8. Shen, L., Ford, J., Makedon, F., Saykin, A.: surface-based approach for classification of 3d neuroanatomical structures. Intelligent Data Analysis 8, 519–542 (2004)
9. Vorperian, H.K., Wang, S., Schimek, E.M., Durtschi, R.B., Kent, R.D., Gentry, L.R., Chung, M.K.: Developmental sexual dimorphism of the oral and pharyngeal portions of the vocal tract: an imaging study. JSLHR 54, 995–1010 (2011)